Geomechanics and Engineering, *Vol. 36, No. 1 (2024) 27-37*
https://doi.org/10.12989/gae.2024.36.1.027

Stability analysis of roof-filling body system in gob-side entry retained

Jinlin Xin[1], Zizheng Zhang*[1,2], Weijian Yu[1] and Min Deng[1]

[1]*Key Laboratory of Coal Mine Gas and Roof Disaster Prevention and Control, Hunan University of Science and Technology, Xiangtan, Hunan 411201, China*
[2]*State Key Laboratory of Mining Response and Disaster Prevention and Control in Deep Coal Mines, Anhui University of Science and Technology, Huainan 232001, China*

(*Received August 18, 2021, Revised November 20, 2023, Accepted November 28, 2023*)

Abstract. The roof-filling body system stability plays a key role in gob-side entry retained (GER). Taking the GER of the 1103 belt transportation roadway in Heilong Coal Mine as engineering background, stability analysis of roof-filling body system was conducted based on the cusp catastrophe theory. Theoretical results showed that the current design parameters of 1103 belt transportation roadway could ensure the roof-filling body system stable during the resistance-increasing support stage of the filling body and the stable support stage of the filling body. Moreover, a verified global numerical model in FLAC3D was established to analyze the failure characteristics including surrounding rock deformation, stress distribution, and plastic zone. Numerical simulation indicated that the width-height ratio of the filling body had a great influence on the stability of the roof-filling body system. When the width-height ratio was greater than 0.62, with the decrease of the width-height ratio, the peak stress of the filling body gradually decreased; when the width-height ratio was greater than 0.92, as the distance to the roadway increased, the roof stress increased and then decreased. The theoretical analysis and numerical simulation findings in this study provide a new research method to analyze the stability of the roof-filling body system in GER.

Keywords: cusp mutation; gob-side entry retained; numerical simulation; roof-filling body system; stability analysis

1. Introduction

The technology of gob-side entry retained (GER) has been widely used in China and other countries (Zhang *et al*. 2021, Yang *et al*. 2020, Smart and Haley 1987). Due to the important influence of the roof above the filling area on the successful implementation of GER, the failure characteristics and stability analysis of the roof-filling body in GER have become one of the key research contents. The successful implementation of GER with roadside filling is the result of the combined effect of the roadway support and the roadside support. Up to now, roadside support has undergone the development process of wood piles, dense pillars, gangue belts, concrete blocks, and high-water materials. The roadway support has undergone the process of wooden shed support, I-steel frame support, U-shaped steel retractable metal support, and anchor mesh cable support. The GER application has also been successful from thin coal seams to thick coal seams, from near-level to gently inclined coal seams (Liu *et al*. 2018, Tan *et al*. 2019).

In recent years, scholars at home and abroad have obtained rich research results and conclusions on the stability of surrounding rock in GER. Han *et al*. (2018) proposed that gob-area roof rupture movement is a key disturbance factor for gob-side entry retaining. Kong *et al*. (2021) analyzed the load-bearing structure of the filling body and top coal in GER of a fully mechanized caving face. Wang *et al*. (2016) proposed and verified the X-type failure principle of the filling body through numerical simulation and experiments. Guo *et al*. (2020) established a mechanical model of the roadside filling support and showed that the fill body must have the longitudinal deformation ability to adapt to the roof subsidence. Chang *et al*. (2018) showed that as the width of the filling body increases, the deformation of the filling body decreases, and the bearing capacity increases by using theoretical analysis and FLAC3D numerical simulation. Li *et al*. (2020) studied the early and late stress states of the filling body formed by the high-water filling materials in Xin'an Coal Mine. At present, most of the scholars focus on the analysis of the roof or the filling body independently. The independent stability analysis of the roof and the filling body has been relatively complete. However, many scholars have not analyzed the filling body and the roof as a whole system, and further analysis is demanded to study the failure characteristics and instability law of the roof-filling body system in GER.

However, the failure characteristics and instability law of surrounding rocks such as coal mine roofs and filling bodies have significant non-linear characteristics, manifested as progressive failure modes, disorder to order, and deformation from constant velocity to non-linear acceleration and jump development. Cusp catastrophe theory is a branch of non-linear theory, which is usually used to analyze rock mass stability problems (Wang *et al*. 2021, Chau 1995). Cusp catastrophe theory focuses on studying the external control conditions when the system state changes suddenly. It explains why some variables in the system change continuously and gradually lead to the

*Corresponding author, Associated Professor
E-mail: 1010096@hnust.edu.cn

ISSN: 2005-307X (Print), 2092-6219 (Online)

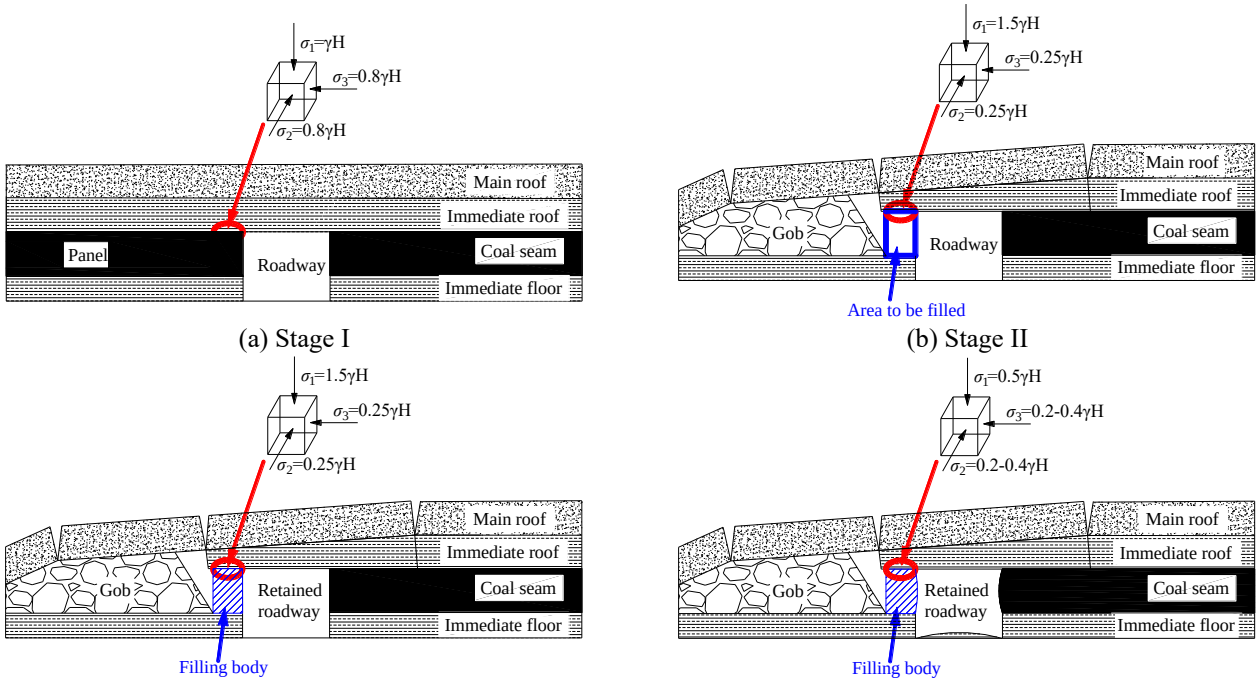

Fig. 1 Multiple stages of roof movement in GER

sudden change of the system state. Fu *et al.* (2018) used the cusp catastrophe theory to study the stability and evolution indexes of gobs under unloading effect in the deep mines.

The above-mentioned study on the stability of surrounding rock in mining engineering based on the cusp catastrophe theory guides for the research on the instability mechanism of the roof-filling body system in GER.

Therefore, a case study in the Heilong Coal Mine was analyzed to the failure characteristics and stability analysis of the roof-filling body system in GER from numerical simulation and theoretical analysis. It is hoped that this engineering stability analysis case can offer an insight into the roof-filling body system failure mechanism with different geological conditions and help to select a reasonable filling body ratio of width to height in GER application.

2. Roof-filling body system failure characteristics in GER

The roof-filling body system in GER has experienced multiple stages of roof movement. According to the fracture characteristics of the roof movement and the resistance-increasing characteristics of the filling body, the deformation of the roof-filling body system in GER can be divided into the original rock stress stage, the advanced abutment stress stage, the resistance-increasing support stage of the filling body, and the stable support stage of the filling body, as shown in Fig. 1.

Stage I (Fig. 1(a)) : The original rock stress stage. At this stage, the roof above the area to be filled is basically in the original rock stress state.

Stage II (Fig. 1(b)) : The advanced abutment stress stage. Due to the advanced abutment stress of the working face, the roof and coal seam in front of the working face is under the action of the concentrated stress. Due to the superposition of lateral abutment stress and original rock stress, the main roof would break above the solid coal.

Stage III (Fig. 1(c)) : The resistance-increasing support stage of the filling body. In the initial filling stage, the strength of the filling body is low. After the filling body is loaded, the roof-filling body integral system is gradually formed. The roof above the filling area can withstand greater pressure and maintain integrity is the guarantee of GER. Due to the continuous increase in the strength of the filling body, the stress of the roof is reduced, and the roof-filling body system tends to be stable.

Stage IV (Fig. 1(d)) : The stable support stage of the filling body. Under the conditions of the filling body support resistance, the stress of the immediate roof, and the roadway support resistance, the roof-filling body system reaches a balanced state, and the retained roadway reaches a stable stage.

3. Engineering sites

The Heilong Coal Mine selected for this case study is located in Shanxi Province, China. The retained roadway is the 1103 working face belt transportation roadway. The belt transportation roadway is 425 m long, 4.5 m wide, and 2.3 m high. It is excavated along the roof of the coal seam. No. 2 coal seam is mainly mined in 1103 working face, with an average thickness of 1.3 m and an average inclination angle

of 14°. The length of the 1103 working face is 151 m. The average buried depth of the working face is 210 m. The north of the 1103 working face is the gob of the 1101 working face, the west is the FS1 reverse fault, and the south is the designed 1105 working face. The immediate roof is mudstone (1.1 m) and the main roof is fine sandstone (3.4 m); the immediate floor and the main floor are both mudstones, with thicknesses of 2.8 m and 3.0 m, respectively.

After mining out the 1103 working face, the 1103 working face belt transportation roadway is retained as the 1105 working face air-return roadway. The retained width of GER is 4.5 m, and the width of the filling body is designed to be 1.2 m. It is constructed by using high-water quick-setting materials with a water-cement ratio of 1.5:1. The single hydraulic props are used to strengthen the roadway support within 80 m behind the active working face. Each row has 3 single hydraulic props. The row spacing is 1000 mm, the column spacing is 1200 mm. and the distance of the side props to the rib is 800 mm, and the top beam is arranged along the width of the roadway.

4. Stability mechanism of roof-filling body system based on cusp catastrophe model

4.1 Stability discrimination of the roof-filling body in GER based on cusp catastrophe model

Catastrophe theory uses topology and singularity theory as mathematical tools to study various mutations. That is to use mathematical models to discuss the universal law of jumpy changes in the state of the system. The main method is to summarize various phenomena into different types of topological structures and discuss the discontinuous characteristics near various critical points. The key to applying catastrophe theory is to establish an appropriate model according to the research problem. Thom (1975) pointed out that when the control variable is not greater than 4 and the state is not greater than 2, there can be up to 7 basic catastrophe models. Among them, the cusp catastrophe model is the most widely used, which has 2 control variables and one state variable. The standard form of its potential function is shown in Eq. (1).

$$V(x)=\frac{1}{4}x^4+\frac{1}{2}mx^2+nx+C \tag{1}$$

Where, x is the state variable of the system; m and n are control variables; (m, n) is the control plane, and (x, m, n) constitutes a three-dimensional space.

Therefore, the steps to use the cusp catastrophe model to analyze the instability of the roof-filling body system in GER are as follows:

(a) Establishing a mechanical model according to the stress environment of the roof-filling body system in GER, finding the total potential energy of the system, establishing the expression of the potential function, and using mathematical methods to transform it into the standard form of the cusp mutation in Eq. (1);

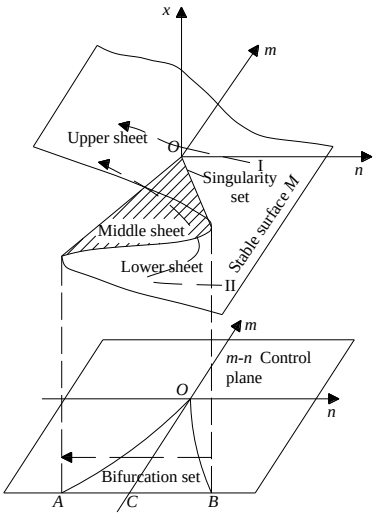

Fig. 2 The balanced surface and bifurcation set of the cus p catastrophe model

(b) Taking the derivative of the potential function $V(x)$, the equation of the balance surface and the equation of the singular point value of the system are shown in Eqs. (2) - (3).

$$V'(x)=x^3+mx+n=0 \tag{2}$$

$$V''(x)=3x^2+n=0 \tag{3}$$

(c) The Eqs. (2) and (3) are eliminated simultaneously to obtain the bifurcation set equation of the system mutation as shown in Eq. (4).

$$\Delta_0=4m^3+27n^2=0 \tag{4}$$

The set of critical points determined by Eq. (4) is the balanced surface. The graph in the (x, m, n) space is composed of the upper, middle, and lower three sheets. The upper and lower sheets are stable, and the middle sheet is not stable. No matter which path m and n change along, the phase point (x, m, n) changes only in the upper sheet (or lower sheet) in a balanced manner. When it reaches the edge of the sheet, it jumps over the middle sheet. Therefore, the points with vertical tangents on the balance surface constitute the set of mutation points of the state. Fig. 2 is a schematic diagram of the balanced surface and bifurcation set of the cusp catastrophe model.

The bifurcation set divides the control variable plane into 2 areas. In the smaller area, the system has 3 equilibrium points, including 2 stable points and one unstable point. In the other larger area, there is only one stable equilibrium point. Thus,

(a) When $\Delta_0>0$, Eq. (4) has only one real number root, which corresponds to a stable equilibrium state, the system deformation is continuous, and the system is in a stable state at this time.

(b) When $\Delta_0<0$, Eq. (4) has 3 real number roots, corresponding to 3 equilibrium states. At this time, the control point has crossed the bifurcation set, and the system is in an unstable state at this time.

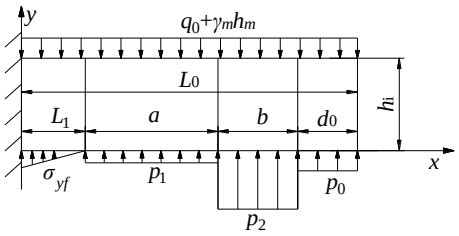

Fig. 3 Mechanical model of the roof-filling body system

(c) When Δ_0=0, Eq. (4) has 3 real number roots, among them, 2 stable states and 1 unstable state. When the control point set (m, n) crosses the boundary of the bifurcation set, it jumps from one branch to another, and the system state changes suddenly.

4.2 Cusp catastrophe model of the roof-filling body system in GER

Based on the cusp catastrophe theory, the stability mechanism of the roof-filling body system in GER is analyzed. First, a mechanical model is established to obtain the standard form of the cusp catastrophe of the system potential function, and then the equilibrium surface and the bifurcation set equation are calculated, and finally obtained conditions for system stability. The upper boundary of the immediate roof in GER is the overlying strata load q_0 and the weight of the main roof. The lower boundary is the support load p_1 in the roadway, the support load p_2 of the filling body, the support stress σ_{yf} of the immediate roof in the limit equilibrium zone, and the temporary support load p_0 outside the filling area. The mechanical model of the roof-filling body system is shown in Fig. 3.

The deflection curve equation $w_i(x)$ of the immediate roof in GER can be obtained by Zhang (2016) as shown in Eq. (5).

$$w_i(x)=\frac{2p_0d_0(L_0-0.5d_0-x)^3+p_2(L_1+a+b-x)^4-(q_0+\gamma_m h_m)(L_0-x)^4}{24E_iI_i}+Cx+D,\quad x\in[L_1+a,\ L_1+a+b] \tag{5}$$

Where,

$$C=\frac{bp_2(L_1+a+0.5b)^2}{4E_iI_i}+\frac{ap_1(L_1+0.5a)^2}{4E_iI_i}+\frac{d_0p_0(L_0-0.5d_0)^2}{4E_iI_i}+\frac{p_xL_1^3}{24E_iI_i\lambda}-\frac{(q_0+\gamma_m h_m)L_0^3}{6E_iI_i}$$

$$D=\frac{(q_0+\gamma_m h_m)L_0^4}{24E_iI_i}-\frac{bp_2(L_1+a+0.5b)^3}{12E_iI_i}-\frac{ap_1(L_1+0.5a)^3}{12E_iI_i}-\frac{d_0p_0(L_0-0.5d_0)^3}{12E_iI_i}-\frac{p_xL_1^4}{120E_iI_i\lambda}$$

$$L_1=\frac{h_d\lambda}{2\tan\varphi_f}\ln\left(\frac{k_0\gamma H_0+\frac{c_f}{\tan\varphi_f}}{\frac{c_f}{\tan\varphi_f}+\frac{p_x}{\lambda}}\right)$$

Where, E_i is the elastic modulus of the immediate roof; I_i is the inertia moment of the cross-section of the immediate roof beam per unit width, $I_i=(h_i)^3/12$; hi is the thickness of the immediate roof; d_0 is the width of temporary support outside the filling area; p_0 is the temporary support strength in the area; p_x is the coal rib support strength; γ_m is the bulk density of the main roof; h_d is the thickness of the coal seam; λ is the lateral pressure coefficient of the coal rib; k_0 is the stress concentration coefficient of the coal rib; γ is the average bulk density of the overlying strata; H_0 is the buried depth of the coal seam; c_f is the cohesion of the coal seam; φ_f is the internal friction angle of the coal seam.

Therefore, when $x=L_1+a+0.5b$, the deflection of the filling body is u (the immediate roof deflection is $-u$), which can be obtained by substituting into Eq. (5).

$$-u=\frac{p_0d_0^4}{96E_iI_i}-\frac{(q_0+\gamma_m h_m)d_0^4}{24E_iI_i}+C(L_1+a+0.5b)+D \tag{6}$$

The filling body of the 1103 belt transportation roadway is constructed by using high-water quick-setting materials, and the filling body has the characteristics of strain softening. Therefore, using the Weibull distribution model (Kim *et al*. 2019), the constitutive relationship of the filling body strain-softening can be expressed as shown in Eq. (7).

$$\left.\begin{aligned}\sigma&=E_b\varepsilon e^{(-\varepsilon/\varepsilon_0)}\\ \varepsilon&=u/h_d\\ \varepsilon_{\max}&=u_{\max}/h_d\end{aligned}\right\} \tag{7}$$

Where, E_b is the elastic modulus of the filling body; ε is the compressive strain; u is the compression displacement of the filling body, which is the same as the sinking displacement of the immediate roof; $\varepsilon_{\max}$ is the strain at the peak point in the stress-strain curve; $u_{\max}$ is the compression displacement of the filling body corresponding to the peak point.

The force balance condition (balance surface) can be obtained shown in Eq. (8) by applying V'=0.

$$\frac{dV}{du}=F_0ue^{(-u/u_{\max})}+480E_iI_iu-G_0 \tag{8}$$

Where, $F_0=-80E_bb^2(L_1+a+0.5b)^3$,

$$G_0=5p_0d_0\left[d_0^3+24(L_1+a+0.5b)(L_0-0.5d_0)^2-8(L_0-0.5d_0)^3\right]+20(q_0+\gamma_m h_m)\left[L_0^4-d_0^4-4L_0^3(L_1+a+0.5b)\right]$$
$$+40ap_1(L_1+0.5a)^2(2L_1+2.5a+1.5b)+\frac{4p_xL_1^3}{\lambda}(4L_1+5a+2.5b)$$

The sharp point can be obtained according to the smooth properties of the balance surface. At the cusp, V'''=0 (see Eq. (9))

$$V'''=80E_bb^2(L_1+a+0.5b)^3\left(\frac{ue^{(-u/u_{\max})}}{u_{\max}^2}-\frac{2e^{(-u/u_{\max})}}{u_{\max}}\right)=0 \tag{9}$$

Therefore, $u_1=2u_{\max}$. At the cusp, the cusp is just the inflection point of the constitutive relationship curve of the filling body in the elastic-plastic zone.

By performing Taylor expansion on the state variable u1 of the balance surface at the cusp, and taking it to the third-degree term, the result is shown in Eq. (10).

$$\begin{aligned}&F_0u_1e^{(-u_1/u_{\max})}+480E_iI_iu_1-G_0\\&+\left[F_0e^{(-u_1/u_{\max})}\left(1-\frac{u_1}{u_{\max}}\right)-480E_iI_i\right](u-u_1)\\&+F_0\frac{e^{(-u_1/u_{\max})}}{2u_{\max}}\left(\frac{u_1}{u_{\max}}-2\right)(u-u_1)^2\\&+F_0\frac{e^{(-u_1/u_{\max})}}{6u_{\max}^2}\left(3-\frac{u_1}{u_{\max}}\right)(u-u_1)^3=0\end{aligned} \tag{10}$$

By introducing the dimensionless state variable z, that is

$$z=(u-u_1)/u_1 \tag{11}$$

The equilibrium surface equation in the standard form of the cusp catastrophe theory can be obtained as shown in Eq. (12).

$$z^3+mz+n=0 \tag{12}$$

Where, $m=\frac{3}{2}\left(-1-\frac{720E_iI_ie^2}{F_0}\right)=\frac{3}{2}(\eta-1)$,

$n=\frac{3}{2}\left(1+\frac{720E_iI_ie^2}{F_0}-\frac{G_0e^2}{2F_0u_{\max}}\right)=\frac{3}{2}(1-\eta+\xi)$,

$$\eta=\frac{3e^2E_ih_i^3}{4E_bb^2(L_1+a+0.5b)^3},\ \xi=\frac{e^2G_0}{-2F_0u_{\max}}.$$

Where, z represents the state variable; m, n represents the control variable; η is the stiffness ratio, that is, the ratio of the roof stiffness and the filling body; the parameter ξ is related to F_0, G_0, and the deformation value $u_{\max}$ at the inflection point, which is called geometric mechanical parameters. It can be seen that the control variables m and n of the system are completely determined by the stiffness ratio η and the geometric mechanical parameters ξ.

The projection of the balanced surface on the m-n plane is the bifurcation set, and the equation is shown in Eq. (13).

$$\Delta_0=4m^3+27n^2=-\frac{27}{2}(\eta-1)^3+\frac{243}{4}(1-\eta+\xi)^2=0 \tag{13}$$

4.3 Stability analysis of the roof-filling body system in GER

4.3.1 Necessary condition for the stability of the roof-filling body system in GER

Generally, there are gradual changes and sudden changes in the destruction of the filling body. When Eq. (13) is satisfied, the filling body becomes unstable and changes along the path II in Fig. 2, and when it reaches the left branch, the slight change of the control variable will cause a sudden change in the system state. At this time, only when m is less than 0, the system can undergo a sudden change across the bifurcation set. Therefore, the necessary condition for the stability of the roof-filling body system in GER is that the stiffness ratio η is greater than 1.

$$\eta=\frac{3e^2E_ih_i^3}{4E_bb^2(L_1+a+0.5b)^3}>1 \tag{14}$$

The stiffness ratio is completely determined by the internal properties of the system (geometrical dimensions, material properties, etc.).

4.3.2 Sufficient condition for the stability of the roof-filling body system in GER

When the roof-filling body system is in the lower sheet, the elastic energy increases, and the system is in a balanced state. With the implementation of the roadway retention, the softening characteristics of the filling body increase, and the roof elastic modulus decrease to the critical state of the middle sheet. When the roof elastic modulus reaches the upper sheet, the system returns to a stable state. The instability process of the filling body is the jumping process of the system from the lower sheet to the upper sheet, that is, the process from $\eta>1$ to $\eta\le1$. When the control variable is disturbed, it exceeds the critical value. Then it jumps from the left branch to the right branch, the roof-filling body system will suddenly lose stability, that is, the roof-filler system will undergo a sudden change. But the sudden change at this time is only the sudden change of the mathematical structure of the system, and the system state variable z does not jump suddenly. When the roof-filling body system is unstable, its deformation tends to increase instantaneously, which corresponds to the situation of crossing the left branch of the bifurcation set ($n<0$). Therefore, the sufficient condition for the instability of the roof-filling body system is summarized as shown in Eq. (15).

$$\left.\begin{aligned}&-\frac{27}{2}\left(\frac{3e^2E_ih_i^3}{4E_bb^2(L_1+a+0.5b)^3}-1\right)^3+\frac{243}{4}\left(1-\frac{3e^2E_ih_i^3}{4E_bb^2(L_1+a+0.5b)^3}+\frac{e^2G_0}{-2F_0u_{\max}}\right)^2=0\\&1-\frac{3e^2E_ih_i^3}{4E_bb^2(L_1+a+0.5b)^3}+\frac{e^2G_0}{-2F_0u_{\max}}<0\end{aligned}\right\} \tag{15}$$

Conversely, to keep the roof-filling body system in GER to be in a stable state, it must be ensured that the control point does not cross the bifurcation set, that is when $\Delta_0>0$. Eq. (16) can be obtained as follows.

$$\begin{aligned}&-\frac{27}{2}\left(\frac{3e^2E_ih_i^3}{4E_bb^2(L_1+a+0.5b)^3}-1\right)^3=\\&-\frac{243}{4}\left(1-\frac{3e^2E_ih_i^3}{4E_bb^2(L_1+a+0.5b)^3}+\frac{e^2G_0}{-2F_0u_{\max}}\right)^2<0\end{aligned} \tag{16}$$

Combining Eq. (14) with Eq. (16), it can be clear that the sufficient and necessary conditions for roof-filling body system instability in GER are consistent.

It can be seen that the stability of the roof-filling body system is not only related to the thickness and elastic modulus of the immediate roof, the elastic modulus of the filling body but also related to the width of the retained roadway, the width of the filling body and the width of the plastic zone of the coal rib.

4.4 Energy-releasing mechanism of catastrophic instability of roof-filling body system in GER

When $m=0$, the balance surface equation has triple zero roots. Under the condition that the bifurcation set equation holds, when $m<0$, there are 3 real roots, namely z_1 , z_2 , z_3 and $z_2=z_3$. When crossing the bifurcation set, the amount of sudden jump of the state variable Δ_z is shown in Eq. (17).

$$\Delta z=z_1-z_2=\frac{3\sqrt{2}}{2}\sqrt{1-\frac{3e^2E_ih_i^3}{4E_bb^2(L_1+a+0.5b)^3}} \tag{17}$$

When the roof-fill body system in GER is in the lower sheet, the system is in a stable equilibrium state. With the progress of working face mining and roadside filling construction, the balance point of the system reaches the crease. Then, as long as it is slightly disturbed, the balance point will go from the crease to the middle sheet, and the instability of the middle sheet cannot exist. Finally, the

Table 1 Typical values of E_i, E_b, p_1, p_2, and p_3 during two different stages

Stage	E_i (GPa)	E_b (GPa)	p_1 (MPa)	p_2 (MPa)	p_3 (MPa)
Resistance-increasing support stage of the filling body	5	0.1	0.5	1	0.1
Stable support stage of the filling body	1	0.1	0.25	8	0.1

Table 2 Necessary and sufficient conditions for determining the instability of the roof-filling body system in GER during two different stages

Stage	η	Necessary condition for the instability	$1-\frac{3e^2E_ih_i^3}{4E_bb^2(L_1+a+0.5b)^3}+\frac{e^2G_0}{-2F_0u_{max}}$	Sufficient condition for the instability
Resistance-increasing support stage of the filling body	1.149	Not satisfied	0.23	Satisfied
Stable support stage of the filling body	-0.269	Satisfied	0.65	Not satisfied

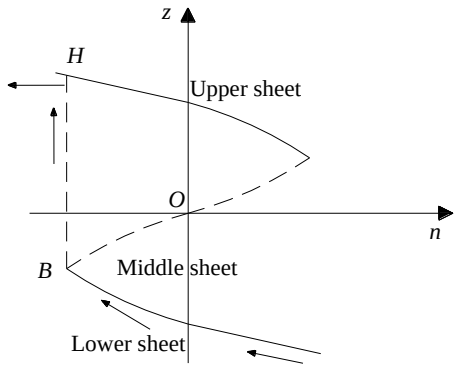

Fig. 4 Sudden jump of state variable z when crossing a bifurcation set

system inevitably jumps to another stable upper sheet, causing the instability process of the system (see Fig. 4). Therefore, the deformation sudden jump before and after the system instability is shown in Eq. (18).

$$\Delta u = u_1\Delta z = 3u_{max}\sqrt{2}\sqrt{1-\frac{3e^2E_ih_i^3}{4E_bb^2(L_1+a+0.5b)^3}} \tag{18}$$

When $\eta\leq1$ and the sudden jump amount meets Eq. (18), system instability will occur. The energy difference of the system before and after the sudden jump can be used to estimate the released energy during the instability process. Expanding the displacement value u_1 relative to the cusp and quoting the dimensionless parameter, the released energy during the instability process can be obtained by Eq. (19).

$$\Delta V = \frac{F_0}{2e^2}u_{max}{}^2(\eta-1)^2 \tag{19}$$

It can be seen that the decrease of the stiffness ratio η means the increase of the released energy. The more the immediate roof stiffness decreases, the more energy the system releases. When the rigidity of the immediate roof remains unchanged, the greater the stiffness of the filling body and the smaller the stiffness ratio η, the more energy the system releases. This is equivalent to the situation where the slope of the softening section becomes steeper, reflecting the brittle nature of the filling body rupture.

4.5 Case analysis

According to the actual production geological conditions and laboratory test results of 1103 belt transportation roadway in GER, H_0=210 m, a=4.0 m, E_b=0.1 GPa, h_d=1.3 m, b=1.2 m, h_m=1.1 m, λ=0.8, q_0=0.15 MPa, k_0=1.5, γ=2.5×10-2 MN/m3, γ_m=2.5×10-2 MN/m3, p_x=0.15 MPa, c_f=1.5 MPa, φ_f=25°, p_1=0.25 MPa, d_0=1 m, p_0=1 MPa. Moreover, according to the mechanical properties of high-water materials (Zhang *et al*. 2020), ε_{max}=0.16.

According to the construction process of the filling body in GER and analyzing the stability of the roof-filling body system, the system can be divided into the resistance-increasing support stage of the filling body and the stable support stage of the filling body. Taking the support strength and roof elastic modulus damage into account in different stages, the typical values of E_i, E_b, p_1, p_2, and p_3 in the above two stages are shown in Table 1.

Incorporating the above results into Eqs. (14)-(16), the necessary and sufficient conditions for determining the instability of the roof-filling body system in GER can be calculated as shown in Table 2.

Therefore, the current design parameters do not meet the necessary condition for the instability of the roof-filling body system in GER during the resistance-increasing support stage of the filling body, and the roof-filling body system will not lose stability at this stage. During the stable support stage of the filling body, the necessary condition for the instability of the roof-filling body system in GER has been met, but the sufficient condition has not been met, and the roof-filling system will not be unstable at this stage.

5. Numerical investigations on roof-filling body failure characteristics subjected to filling body width-height ratio

5.1 Numerical model and simulation plans

Table 3 Strain-softening parameters of the filling body

Plastic parameters	0	0.01	0.06	0.07	0.12	0.14	0.16	1
Cohesion（MPa）	3	3	2.4	1.9	1.75	1.5	1.35	1
Friction（°）	30	30	24	24	24	24	24	16

Table 4 Calculating parameters of the filling body for the strain-softening model

Parameters	Density ($kg \cdot m^{-3}$)	Bulk modulus (GPa)	Shear modulus (GPa)
Value	1100	0.274	0.07

Table 5 Parameters of the rock strata and coal seam

Rock strata	Thickness (m)	Density (kg/m3)	Bulk modulus (GPa)	Shear modulus (GPa)	Cohesion (MPa)	Friction (°)
Main roof	3.4	2670	1.9	1.2	3.2	37
Immediate roof	1.1	2720	1.7	0.94	1.42	20
Coal	1.4	1400	1.1	0.73	2.1	16
Immediate floor	2.8	2680	1.9	0.93	1.5	24
Main floor	3	2700	2.4	1.2	4.2	41

FLAC^{3D} software has been widely used to simulate the impact of coal mining stress, so it can be used to analyze the stability of the surrounding rock in GER (Lee *et al*. 2021, Kim *et al*. 2019, Kwon and Lee 2018, Wang *et al*. 2018, Li *et al*. 2020). According to the mining and geology conditions of the 1103 working face, the plane strain numerical simulation model shown in Fig. 5 was established. The model included the main floor (3 m), immediate floor (2.8 m), 2# coal (1.3 m), and immediate roof (1.1 m), the main roof (3.4 m). Meanwhile, considering the boundary effect, 20 m above and 20 m below the model were added to simulate the overlying strata and underlying strata, respectively. The overall size of the model was 145.2 m×2 m×51.6 m (length×width×height), a total of 4374 zones and 6888 nodes. The bottom of the model was fixed without displacement, and the normal displacement of the boundary was limit. On the top of the model, a vertical load of 4.605 MPa was applied to simulate the weight of the overburden. According to the distribution law of ground stress, the lateral pressure coefficient was set to 0.8. The roadside filling body was constructed by using high-water quick-setting materials with a water-cement ratio of 1.5:1.

The filling body has obvious plastic characteristics, so the strain-softening model was used to simulate the roadside filling body. The Mohr-Coulomb model was used to simulate the roof and floor strata. To evaluate the influence of the gob stress recovery and the bearing characteristics of the caving zone on the mining abutment stress of longwall mining, the Double-Yield model is often used in FLAC^{3D} to simulate the strain-hardening characteristics of the gob materials.

According to the literature (Zhang 2016), it can be known that the strain-softening parameters of the filling body in the FLAC^{3D} simulation are shown in Tables 3 and 4. The detailed parameters of the rock strata and coal seam are shown in Table 5.

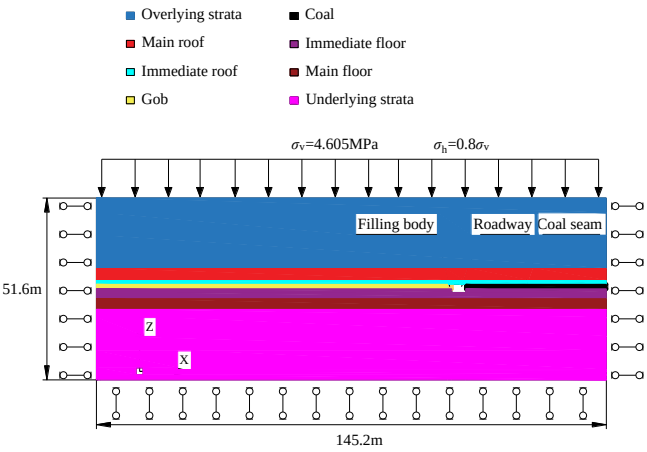

Fig. 5 Roof-filling body system numerical model

5.2 Parameter determination and model verification of the Double-Yield constitutive model for gob materials

5.2.1 Parameter determination of the Double-Yield constitutive model for gob materials

The load-bearing capacity of the gangue in the gob of the working face has a greater influence on the distribution law of the mining abutment stress. The greater the load-bearing capacity, the smaller the mining abutment stress appears. Many scholars believe that the vertical stress at the edge of the gob is basically zero and gradually increases toward the middle of the gob until the in-situ stress level. When the distance to the gob was 0.12 to 0.6 times the depth of the coal seam, the stress in the gob was the original rock stress. As the depth of the coal seam was deeper, when the gob stress recovered, the closer it was to the edge of the gob; the materials in the gob showed the characteristic of strain hardening. Therefore, the initial model parameters were obtained using the Salamon's model (Eq. (20)) (Bali and Mishra 2021, Yadav *et al*. 2020, Esterhuizen *et al.* 2010, Morsy and Peng 2002).

$$\left.\begin{aligned} \sigma_g &= \frac{E_{g0}\varepsilon_g}{1-\varepsilon_g/\varepsilon_{gmax}}, \quad \varepsilon_{gmax} = \frac{b_g-1}{b_g} \\ b_g &= \frac{h_{cav}+h_m}{h_{cav}}, \quad E_{g0} = \frac{10.39\sigma_{cg}^{1.042}}{b_g^{7.7}} \end{aligned}\right\} \tag{20}$$

Where, b_g is the expansion coefficient of the gangue; ε_{gmax} is the maximum strain of the gob materials; h_{cav} is the height of the caving zone; hm is the mining thickness of the coal seam; σ_{cg} is the initial vertical stress at the top of the coal seam; E_{g0} is the initial modulus of the gob materials.

In practice, the height of the caving zone is generally 2-8 times the mining thickness of the coal seam. According to the geological conditions of the 1103 working face, the coal

Table 6 Stress-strain relationship of the gob materials

Strain (m/m)	Stress (MPa)	Strain (m/m)	Stress (MPa)	Strain (m/m)	Stress (MPa)
0.01	0.1	0.08	1.1	0.15	4.24
0.02	0.21	0.09	1.41	0.16	5.23
0.03	0.32	0.10	1.69	0.17	6.58
0.04	0.46	0.11	2.02	0.18	8.55
0.05	0.6	0.12	2.41	0.19	11.66
0.06	0.77	0.13	2.89	0.20	17.36
0.07	0.95	0.14	3.49	0.21	31.13

Table 7 main mechanical parameters of the Double-Yield model

Parameters	Density ($kg \cdot m^{-3}$)	Bulk modulus (GPa)	Shear modulus (GPa)	Friction (°)	Dilatancy angle (°)
Value	1800	6.8	5.53	24	7

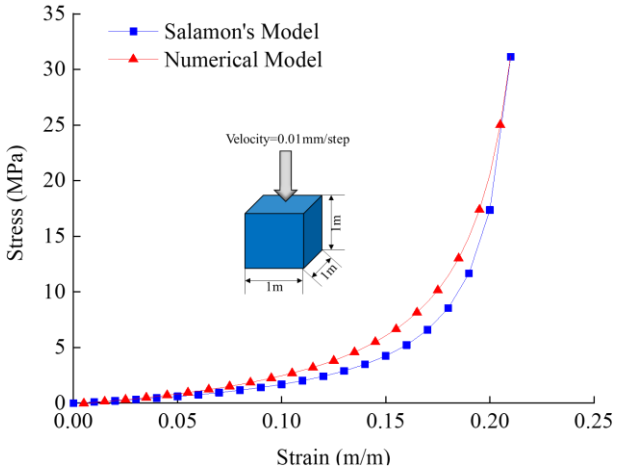

Fig. 6 Comparison result of the stress-strain relationship between the gob materials in the numerical model and the Salamon's model

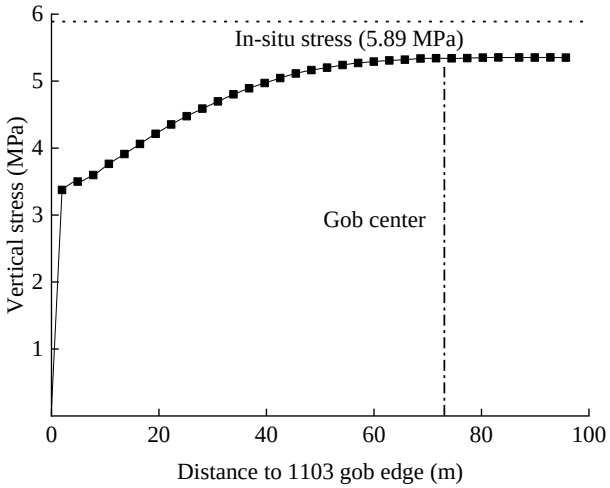

Fig. 7 Vertical stress distribution of 1103 gob

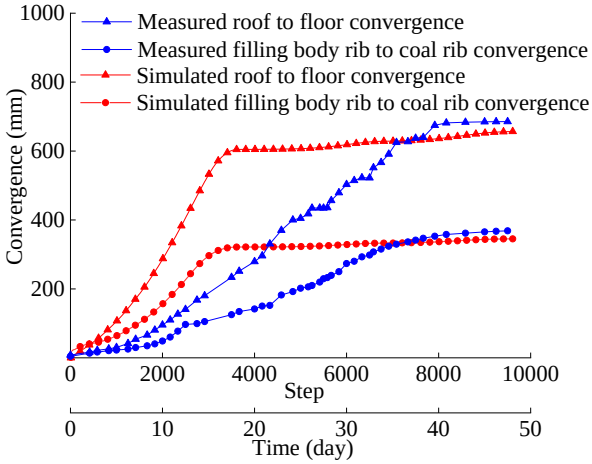

Fig. 8 comparison of the actual measured surrounding rock deformation with the deformation obtained by the numerical simulation

seam mining thickness was 1.3 m, and the height of the caving zone was 4.5 m. Substituting the Eq. (20). It can be calculated that the expansion coefficient of the gob materials was 1.289, the maximum strain was 0.22, the initial vertical stress at the top of the coal seam was 5.895 MPa, the initial modulus of the gob materials was 9.35 GPa. The stress-strain relationship of the gob materials was shown in Table 6.

To determine the reasonableness and accuracy of other parameters of the Double-Yield model in FLAC^{3D}, the unique element method was used for parameter verification. The unit block size was 1m×1m×1m, the displacement was fixed at the periphery and bottom of the model, and a fixed vertical velocity was applied to the top of the model. The main mechanical parameters of the Double-Yield model for the gob materials in FLAC^{3D} were obtained by the trial-and-error method inversion. The main mechanical parameters were as follows as shown in Table 7, the comparison result of the stress-strain relationship between the gob materials in the numerical model and the Salamon's model was shown in Fig. 6.

To verify the rationality of the parameters of the Double-Yield constitutive model for gob materials, the vertical stress data of the 1103 gob at the central height of the coal seam was recorded and extracted to obtain the vertical stress distribution law of 1103 gob as shown in Fig. 7. This curve was compared with existing research results.

It can be seen that the vertical stress at the edge of the 1103 gob was zero; as the distance to the edge of the gob increased, the vertical stress in the gob increased rapidly. When the distance to the edge of the gob was 50 m, the vertical stress reached 5.19 MPa. That is, when the 1103 gob was restored to the in-situ stress of 88.1% (5.19 MPa/5.89 MPa), the depth of the coal seam at this distance was 21.2% (50 m/235.8 m), which was consistent with the results of other scholars. Therefore, the Double-Yield model and its parameters used in this model are appropriate.

5.3 Global model verification

To verify the rationality of the global model parameters, Fig. 8 showed the comparison of the actual measured surrounding rock deformation with the deformation

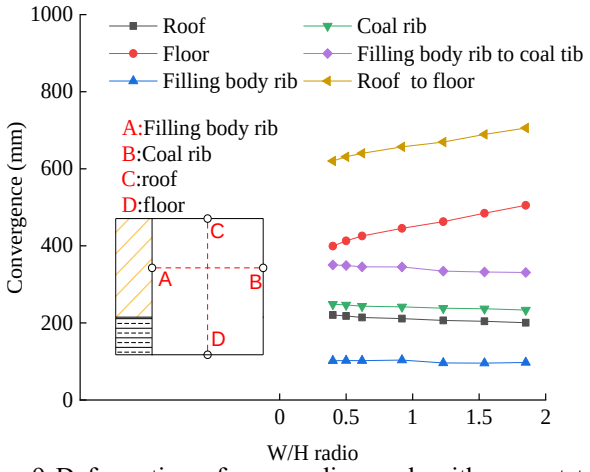

Fig. 9 Deformation of surrounding rock with respect to different width-height ratios

obtained by the numerical simulation. The actual measured results were obtained from daily monitoring, and the numerical simulation results were obtained from time steps.

The time steps were corresponding to different measuring times for comparison and analysis. The final roof to floor convergence between the measured results and the numerical simulation results had an error of 4.2%, and the error of the filling body rib to coal rib convergence was 6.3%, the actual monitoring data and simulation results displayed by the two were the same. Therefore, the coal rock parameters used in this paper are appropriate.

5.4 Simulation result analysis

In this study, we focused on the deformation and instability of the roof-filling body system in GER. The width-height ratios of the filling body were selected to be 0.4, 0.5, 0.62, 0.92, 1.23, 1.54, and 1.85, then the deformation, stress of the roof-filling body system, and the plastic zone were analyzed. Fig. 9 showed the deformation of surrounding rock with respect to different width-height ratios.

From Fig. 9, it can be seen that: as the width-height ratio of the filling body increased, the floor heave increased rapidly, the roof subsidence, the filling body rib convergence, and the coal rib convergence decreased slowly, and the roof sinks increased and then decreased; as the width-height ratio of the filling body increased, the convergence of the filling body rib to the coal rib increased and then decreased, and the convergence of the roof to floor gradually increased.

Fig. 10 showed the vertical stress and plastic zone distributions of the roof-filling body system with respect to different width-height ratios.

From Fig. 10, it can be seen that: as the distance to the roadway increased, the stress of the filling body increased rapidly, and the roof stress decreased slowly; when the width-height ratio was greater than 0.62, with the decrease of the width-height ratio, the peak stress of the filling body gradually decreased; when the width-height ratio was greater than 0.92, as the distance to the roadway increased, the roof stress increased and then decreased; as the distance to the roadway increased, the stress increased and then decreased; as the width-height ratio increased, the coal rib stress increased little, the peak stress was located at 10.5 m to 11 m away from the roadway rib.

Meanwhile, it can be seen that: as the width-height ratio increased, the shear failure and tensile failure had always occurred on the filling body close to the retained roadway; when the width-height ratio was greater than 1.54, the internal tensile failure of the filling body decreased and the shear failure increased; as the width-height ratio increased, both the shear failure and tensile failure always occurred on the roof close to the gob. When the width-height ratio of the filling body was greater than 0.92, the roof mainly suffered from shear failure.

6. Conclusions

This paper investigates failure characteristics and stability analysis of the roof-filling body system in GER of Heilong coal mine, China. Theoretical analysis and numerical simulation of the roof-filling body system of in GER of 1103 working face belt transportation roadway were conducted.

Cusp catastrophe model of the roof-filling body system in GER was established to analyze the system stability including the necessary condition and sufficient condition. The necessary condition for the stability of the roof-filling body system in GER is that the stiffness ratio of the roof to the filling body was greater than 1. The sufficient condition for the instability of the roof-filling body system was that the bifurcation set equation of the system was greater than 0. The more the immediate roof stiffness decreased, the more energy the roof-filling body system released. When the rigidity of the immediate roof remained unchanged, the greater the stiffness of the filling body and the smaller the stiffness ratio, the more energy the system released. The current design parameters in GER of 1103 working face belt transportation roadway could ensure the roof-filling body system stable during the resistance-increasing support stage of the filling body and the stable support stage of the filling body.

A global numerical model in FLAC^{3D} was established to analyze the roof-filling body system stability with respect to different width-height ratios of the filling body. The Double-Yield model was used to simulate the strain-hardening characteristics of the gob materials, and the strain-softening model was used to simulate the plastic characteristics of the roadside filling body. The global model and its parameters were verified by comparison the in-site measured surrounding rock deformation data with the simulated data. The numerical simulation results showed that the width-height ratio of the filling body had a great influence on the stability of the roof-filling body system. When the width-height ratio was greater than 0.62, with the decrease of the width-height ratio, the peak stress of the filling body gradually decreased; when the width-height ratio was greater than 0.92, as the distance to the roadway increased, the roof stress increased and then

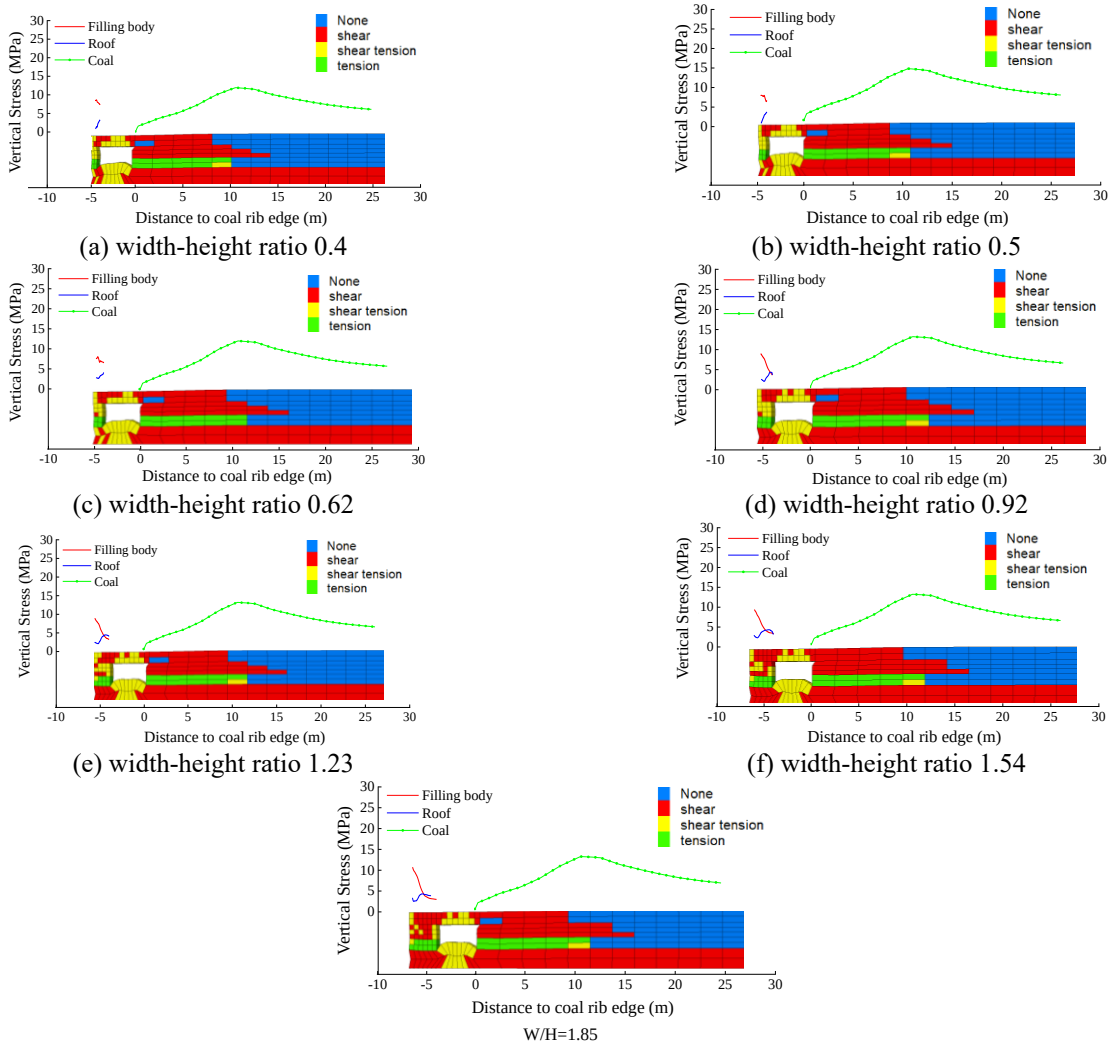

(a) width-height ratio 0.4

(b) width-height ratio 0.5

(c) width-height ratio 0.62

(d) width-height ratio 0.92

(e) width-height ratio 1.23

(f) width-height ratio 1.54

(g) width-height ratio 1.85

Fig. 10 Vertical stress and plastic zone distributions of the roof-filling body system with respect to different width-height ratios

decreased. When the width-height ratio was equal to 0.92, the displacement of the filling body was the largest.

The findings in this study would lead to better understanding of the failure characteristics and stability mechanism of the roof-filling body system in GER and provide a new research method to analyze the stability of the roof-filling body system under similar mining and geological conditions.

Acknowledgments

The project was supported by the Key Research and Development Special Tasks of Xinjiang Province (No. 2022B01051), Key projects of the Joint Fund of the National Natural Science Foundation of China (No. U21A20107), the Open Fund of the State Key Laboratory of Mining Response and Disaster Prevention and Control in Deep Coal Mines, Anhui University of Science and Technology (No. SKLMRDPC20KF08), and Funded by the Excellent Youth Fund of the Education Department of Hunan Province (Grant No. 21B0487).

Availability of data and materials

The datasets used or analyzed during the current study are available from the corresponding author on reasonable request.

Competing interests

The authors have declared that no competing interests exist.

Authors' contributions

Zizheng Zhang and Weijian Yu contributed to the conception of the study; Jinlin Xin and Min Deng contributed significantly to analysis and manuscript preparation; Jinlin Xin performed the data analyses and wrote the manuscript; Zizheng Zhang helped perform the analysis with constructive discussions.

References

Bali, B.A.M. and Mishra, B. (2021), "Determination of suitable pillar size for protecting gas well drilled through a longwall mining abutment pillar using numerical modelling approach: a case study", *Geotech. Geol. Eng.*, **39**(2), 1329-1347. https://doi.org/10.1007/s10706-020-01561-6.

Chang, Q.L., Tang, W.J., Xu, Y. and Zhou, H.Q. (2018), "Research on the width of filling body in gob-side entry retaining with high-water materials", *Int. J. Min. Sci. Technol.*, **28**(3), 519-524. https://doi.org/10.1016/j.ijmst.2017.12.016.

Chau, K.T. (1995), "Landslides modeled as bifurcations of creeping slopes with nonlinear friction law", *Int. J. Solids Structures*, **32**(23), 3451-3464. https://doi.org/10.1016/0020-7683(94)00317-P.

Esterhuizen, E., Mark, C. and Murphy, M.M. (2010), "Numerical model calibration for simulation coal pillars, gob and overburden response", *Proceeding of the 29th International Conference on Ground Control in Mining*, Morgantown, USA, January.

Fu, J.X., Song, W.D. and Tan, Y.Y. (2018), "Study of stability and evolution indexes of gobs under unloading effect in the deep mines", *Geomech. Eng.*, **14**(5), 439-451. https://doi.org/10.12989/gae.2018.14.5.439.

Guo, P.F., Zhang, X.H., Peng, Y.Y., He, M.C., M,a C.R. and Sun, D.J. (2020), "Research on deformation characteristic and stability control of surrounding rock during gob-side entry retaining", *Geotech. Geol. Eng.*, **38**(3), 2887-2902. https://doi.org/10.1007/s10706-020-01194-9.

Han, C.L., Zhang, N., Ran, Z., Gao, R. and Yang, H.Q. (2018), "Superposed disturbance mechanism of sequential overlying strata collapse for gob-side entry retaining and corresponding control strategies", *J. Central South Univ.*, **25**(9), 2258-2271. https://doi.org/10.1007/s11771-018-3911-8.

Kim, B.H. and Larson, M.K. (2019), "Development of a fault-rupture environment in 3D: A numerical tool for examining the mechanical impact of a fault on underground excavations", *Int. J. Min. Sci. Technol.*, **29**(1), 105-111. https://doi.org/10.1016/j.ijmst.2018.11.008.

Kim, J.S., Kim, G.Y., Baik, M.H., Finsterle, S. and Cho, G.C. (2019), "A new approach for quantitative damage assessment of in-situ rock mass by acoustic emission", *Geomech. Eng.*, **18**(1), 11-20. https://doi.org/10.12989/gae.2019.18.1.011.

Kong, D.Z., Pu, S.J., Cheng, Z.H., Wu, G.Y. and Liu, Y. (2021), "Coordinated deformation mechanism of the top coal and filling body of gob-side entry retaining in a fully mechanized caving face", *Int. J. Geomech.*, **21**(4), 04021030. https://doi.org/10.1061/(ASCE)GM.1943-5622.0001972.

Kwon, S. and Lee, C. (2018), "THM analysis for an in situ experiment using FLAC3D-TOUGH2 and an artificial neural network", *Geomech. Eng.*, **16**(4), 363-373. http://dx.doi.org/10.12989/gae.2018.16.4.363.

Lee, C., Lee, J. and Kim, G.Y. (2021), "Numerical analysis of coupled hydro-mechanical and thermo-hydro-mechanical behaviour in buffer materials at a geological repository for nuclear waste: Simulation of EB experiment at Mont Terri URL and FEBEX at Grimsel test site using Barcelona basic model", *Int. J. Rock Mech. Min. Sci.*, **139**, 104663. https://doi.org/10.1016/j.ijrmms.2021.104663.

Li, T., Chen, G.B., Qin, Z.C., Li, Q.H., Cao, B. and Liu, Y.L. (2020), "The gob-side entry retaining with the high-water filling material in Xin\'an Coal Mine", *Geomech. Eng.*, **22**(6), 541-552. https:// doi.org/10.12989/gae.2020.22.6.541.

Liu, X.S., Ning, J.G., Tan, Y.L., Xu, Q. and Fan, D.Y. (2018), "Coordinated supporting method of gob-side entry retaining in coal mines and a case study with hard roof", *Geomech. Eng.*, **15**(6), 1173-1182. https://doi.org/10.12989/gae.2018.15.6.1173.

Li, Z.L., Shan, R.L., Wang, C.H., Yuan, H.H. and Wei, Y.H. (2020), "Study on the distribution law of stress deviator below the floor of a goaf", *Geomech. Eng.*, **21**(3), 301-313. https://doi.org/10.12989/gae.2020.21.3.301.

Morsy, K. and Peng, S. (2002), "Numerical modeling of the gob loading mechanism in longwall coal mines", *Proceeding of the 21th International Conference on Ground Control in Mining*, Morgantown, USA, January.

Smart, B.G.D. and Haley, S.M. (1987), "Further development of the roof strata tilt concept for pack design and the estimation of stress development in a caved waste", *Int. J. Min. Sci. Technol.*, **5**(2), 121-130. https://doi.org/10.1016/S0167-9031(87)90355-0.

Tan, Y.L., Ma, Q., Zhao, Z.H., Gu, Q.H., Fan, D.Y., Song, S.L. and Huang, D.M. (2019), "Cooperative bearing behaviors of roadside support and surrounding rocks along gob-side", *Geomech. Eng.*, **18**(4), 439-448. https://doi.org/10.12989/gae.2019.18.4.439.

Thom, R. (1975), Structural stability and morphogenesis. Reading: W.A. Benjamin, Inc.

Wang, C.L., Li, G.Y., Gao, A.S., Shi, F., Lu, Z.J. and Lu, H. (2018), "Optimal pre-conditioning and support designs of floor heave in deep roadways", *Geomech. Eng.*, **14**(5), 429-437. https://doi.org/10.12989/gae.2018.14.5.429.583.

Wang, H.S., Zhang, D.S., Liu, L., Guo, W.B., Fan, G.W., Song, K. and Wang, X.F. (2016), "Stabilization of gob-side entry with an artificial side for sustaining mining work", *Sustainability*, **8**(7), 627. https://doi.org/10.3390/su8070627.

Wang, X.R., Guan, K., Yang, T.H. and Liu, X.G. (2021), "Instability mechanism of pillar burst in asymmetric mining based on cusp catastrophe model", *Rock Mech. Rock Eng.*, **54**(3), 1463-1479. https://doi.org/10.1007/s00603-020-02313-x.

Yadav, A., Behera, B., Sahoo, K., Singh, G.S.P. and Sharma, S.K. (2020), "Numerical analysis of the gob stress distribution using a modified elastic model as the gob constitutive model", *J. Institution of Engineers (India): Series D*, **101**(1), 127-139. https://doi.org/10.1007/s40033-020-00214-5.

Yang, H.Y., Liu, Y.B., Cao, S.G., Pan, R.K., Wang, H., Li, Y. and Luo, F. (2020), "A caving self-stabilization bearing structure of advancing cutting roof for gob-side entry retaining with hard roof stratum", *Geomech. Eng.*, **21**(1), 23-33. https://doi.org/10.12989/gae.2020.21.1.023.

Zhang, F.T., Wang, X.Y., Bai, J.B., Wang, G.Y. and Wu, B.W. (2020), "Post-peak mechanical characteristics of the high-water material for backfilling the gob-side entry retaining: from experiment to field application", Arabian J. Geosci., **13**(9), 386. https://doi.org/10.1007/s12517-020-05369-9.

Zhang, Z.Z., Deng, M., Bai, J.B., Yan, S. and Yu, X.Y. (2021), "Stability control of gob-side entry retained under the gob with close distance coal seams", Int. J. Min. Sci. Technol., **31**(2), 321-332. https://doi.org/10.1016/j.ijmst.2020.11.002.

Zhang, Z.Z. (2016). Investigation on stability mechanism and control techniques of immediate roof above backfill area in gob-side entry retaining, PhD dissertation, China University of Mining and Technology.

CC